Highly strained graphene ssamples of varying thickness and comparison of their behaviour

Perez-Garza, H.H.; Kievit, E.W.; Schneider, G.F.; Staufer, U.

Highly strained graphene samples of varying thickness and comparison of their behaviour

2014 Nanotechnology 25 465708

(http://iopscience.iop.org/0957-4484/25/46/465708)

OPEN ACCESS
IOP Publishing
Nanotechnology

Nanotechnology **25** (2014) 465708 (9pp)
doi:10.1088/0957-4484/25/46/465708

Highly strained graphene samples of varying thickness and comparison of their behaviour

Héctor Hugo Pérez-Garza[1], Eric Walter Kievit[1], Grégory F Schneider[2] and Urs Staufer[1]

[1] Department of Precision and Microsystems Engineering, Research Group of Micro and Nano-Engineering, Delft University of Technology, Mekelweg 2, 2628 CD, Delft, The Netherlands
[2] Leiden University, Faculty of Science, Leiden Institute of Chemistry, Einsteinweg 55, 2333 CC Leiden, The Netherlands

E-mail: H.H.PerezGarza@tudelft.nl and U.Staufer@tudelft.nl

Received 22 July 2014, revised 17 September 2014
Accepted for publication 29 September 2014
Published 31 October 2014

Abstract

Mechanically straining graphene opens the possibility to exploit new properties linked to the stressed lattice of this two-dimensional material. In particular, theoretical analyses have forecast that straining graphene by more than 10% is a requirement for many novel applications that have not yet been experimentally demonstrated. Recently, we reported having achieved 12.5% strain in a trilayer graphene sample (3LG) in a controlled, reversible and non-destructive way. In this paper, we explore our method by straining samples of varying thicknesses and comparing their behavior, where strains of 14% and 11% were achieved for monolayer and four-layer graphene (4LG), respectively. For the analysis, optical tracking and the correspondent Raman spectra were taken. While doing so, we observed slippage between two layers in a bilayer sample of which one layer was clamped on one side only. The obtained results when stretching different samples to extreme strains demonstrated the exceptional elasticity of graphene, which might be essential for practical applications. Hysteretic effects observed in the partially clamped layer hints at small energy losses during slippage. This may shed new light on the superlubricity property of graphene that has been reported in the literature.

S Online supplementary data available from stacks.iop.org/NANO/25/465708/mmedia

Keywords: graphene, extreme strains, tensile MEMS, clamping, mechanical stress, slippage

(Some figures may appear in colour only in the online journal)

1. Introduction

Since the discovery of graphene [1], this two-dimensional (2D) material has represented a rapidly increasing 'star on the horizon' of material science and nanotechnology [2] because of its unique properties. As a result, scientists have been trying to explore novel opportunities in various fields. Theoretical work has predicted that straining graphene by more than 10% is a prerequisite for many expected applications [3–9]. These include, for example, using graphene as an active and reversible hydrogen storage medium [3, 4], engineering bandgaps [10] in graphene for nano-electronics [6] and optical devices [11], or generating synthetic electromagnetic fields [5]. A full list of the predicted applications of graphene under more than 10% strain can be found in the supplementary data. However, none of these applications have been experimentally demonstrated to their full extend so far, since achieving significant strains in a controlled way has represented a considerable challenge. Previous experimental efforts to strain graphene [7–9, 12–17] demonstrated maximum values of ~4.5% [7, 8, 16, 18], which were still restraining the intended applications. We have recently reported a controlled, reversible and nondestructive way to generate uniaxial

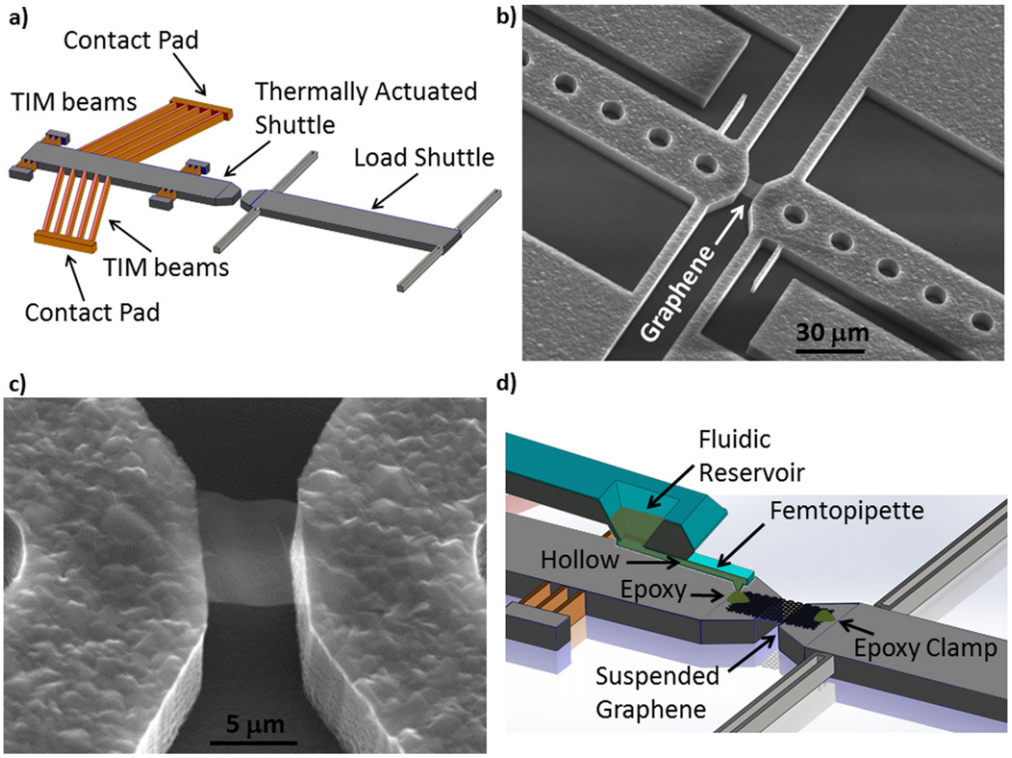

Figure 1. Micro-electro-mechanical System (MEMS) based in-plane tensile device and clamping mechanism. (a) The device consisted of two shuttles, namely the thermally actuated and load shuttles. The first uses a TIM, which relies on an applied power that creates a displacement. When voltage is applied between the contact pads, current flows through the thermal beams, generating heat that makes them expand, inducing a displacement of the shuttle. When the graphene bridges both shuttles, the shuttle displacement results in a pulling effect on the graphene. The TIM could withstand a maximum power of 2.4 W before the beams were plastically deformed, corresponding to a measured temperature of nearly 900 °C. (b) Scanning electron microscopy (SEM) picture of the graphene bridging the shuttles. (c) The zoomed version of the graphene bridge. (d) In order to prevent the graphene from slipping away when experiencing high tensile forces, both edges were locally clamped with epoxy, which was accurately dispensed with the femtopipette. When the tip of the pipette snapped in, a controlled amount of epoxy was deposited. Care was taken to ensure that the temperature at the location of the epoxy clamp did not exceed 40 °C. All details of the clamping method and the chemistry involved, along with the design and characterization of the device, were reported in a separate paper [19].

extreme (>10%) strains in graphene using a microfabricated tensile device [19]. There, we reached a strain of 12.5% on a trilayer graphene (3LG) sample. In this study, we explore our method by straining samples of varying thicknesses and comparing their behavior, where strains of 14% and 11% were achieved for monolayer and four-layer graphene (4LG), respectively. While doing so, we observed slippage between two layers in a bilayer sample of which one layer was clamped on one side only.

The tensile device, briefly, consisted of two suspended beams that were aligned to and movable along a single axis (figure 1(a)). One of the beams could be actively pulled using a thermal in-plane microactuator (TIM), while the other was fixed to calibrated springs, which allowed force measurements. Both beams were then bridged by graphene, as shown in figures 1(b), (c). The graphene was stressed when the TIM was actuated, creating a tensile pulling effect. In most of the previously reported experiments, graphene was placed as a fully suspended membrane, ready to be strained [8, 9, 12, 15]. It has been observed that it slipped away from the surface when the van der Waals adhesion is overcome by the tensile force [9]. Consequently, proper clamping would dramatically increase the chances of achieving higher strains. Therefore, to prevent graphene from slipping away, it was clamped using epoxy patches locally deposited along the two edges of the graphene [19]. To accurately dispense the epoxy, we used a previously developed femtopipette (figure 1(d)) [20, 21]. During stretching, optical images and Raman spectra were taken.

2. Materials and methods

2.1. Graphene transferring

The transfer of graphene, based on previous work [22], was performed using mechanically exfoliated ribbons of different thicknesses. When the flake of interest was found, the oxidised Si-chip, onto which the flakes were originally transferred from adhesive tape, was dipped into a solution of cellulose acetate butyrate in ethyl acetate, which had a ~30 mg mL^{-1} ratio. After dipping, the substrate was removed from the solution and the solvent was allowed to evaporate under ambient conditions. After that, the chip was dipped into water under a ~30 degree angle, allowing the water to enter

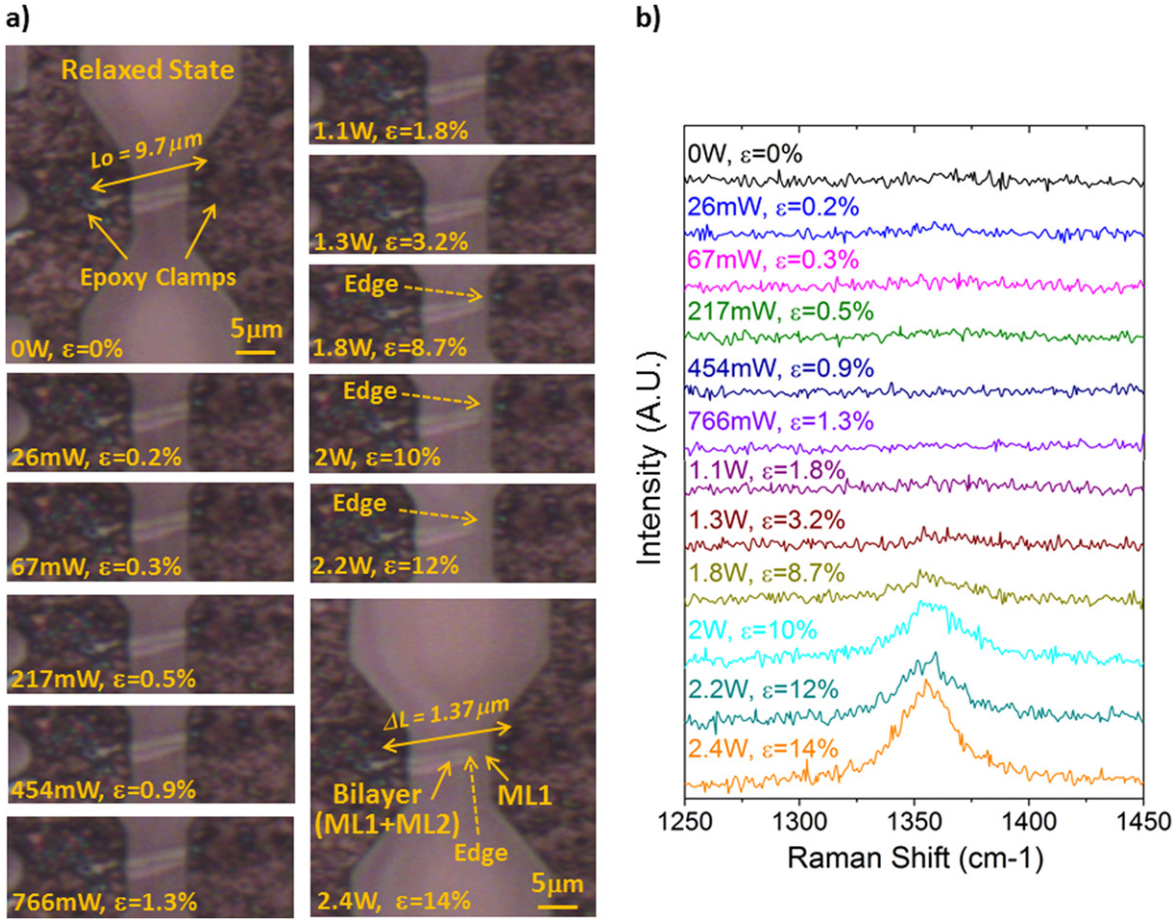

Figure 2. Optical tracking of the bilayer sample during straining. (a) The power was gradually increased from 0 W to 2.4 W, generating forces of up to 330 μN to achieve maximum strain. For each step, the respective optical image was taken. After $\varepsilon = 8.7\%$, an edge appeared within the image, indicating that only one of the monolayers was fully clamped (ML1), while the other slipped. Consequently, only the fully clamped layer experienced the full stress produced by the displacement of the beams. The edge thus corresponded to the other monolayer (ML2) that was effectively clamped only on one side. A video of the graphene sample being stretched up to $\varepsilon = 14\%$ is shown in the supplementary data. This was confirmed with Raman spectroscopy, where the (b) spectra showed the appearance and gradual increase of the D-band as the edge moved towards the center of the laser beam. The laser was focused to a spot size of around 1 μm and was placed in the middle of the ~4 μm wide suspended sample. In order to corroborate that the appearance of D-band was caused by the edge and not because the elongation of the C–C bonds, we stretched another fully clamped sample and saw no increase of the D-band for the same high strains. An additional control experiment for further confirmation is shown in figure 1 of the supplementary data.

through the interface formed between the hydrophobic polymer and the hydrophilic oxide. Due to the differences in surface energies, the polymer came off the substrate, peeling the graphene along with it. This was caused by hydrophobic interactions. When the polymer was floating on the water, a micromanipulator was used to hold it while the MEMS device (placed at the bottom of the beaker filled with water) was becoming aligned relative to the position of the graphene. Once they were aligned, the water was pumped out of the beaker, decreasing the distance between the polymer/graphene and the chip. Once in contact, the polymer was left until it dried out and finally dissolved to release the graphene.

2.2. Clamping the graphene

The clamping of graphene was also based on our previous work [19]. To start with, an epoxy resin was mixed with an amine-containing curing agent. For this experiment, the 353ND epoxy (EpoTek technology) was used, consisting of bisphenol F. A small volume of the freshly mixed epoxy was accurately dispensed on the edges of the graphene using a femtopipette previously developed in our group [20, 21]. To further control the positioning of the femtopipette, it was mounted with 4 degrees of freedom on a robot used for nanomanipulation. The robot, with the femtopipette mounted on the edge of its actuated arm, was placed underneath an optical microscope and remotely controlled.

2.3. Raman analysis

The experimental setup comprised a Horiba Labram HR Raman spectroscope and a probe station. The excitation source was a 532 nm laser with a power below 0.1 mW on the graphene sample to avoid laser-induced local heating. A 50x objective lens (numerical aperture 0.75) was used to focus the laser to a spot size of around 1 μm. The device containing the

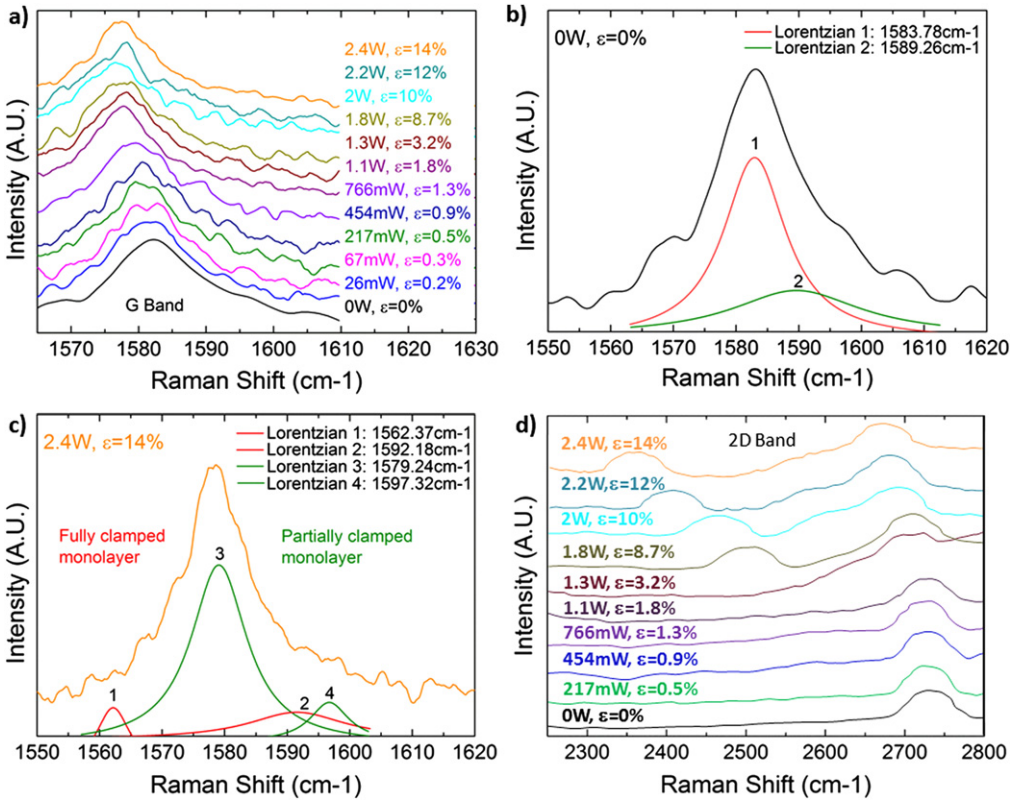

Figure 3. Raman study of bilayer sample and extraction of monolayer information. (a) Raman analysis of the bilayer's G-band evolution as a function of strain. From such analysis, we extracted the individual strains of each monolayer by fitting the Lorenztian peaks inside each band. (b) When relaxed, the G-band showed two Lorenztians with maxima at 1583.8 cm^{-1} and 1589.3 cm^{-1}. (c) At its maximum experienced strain, the G-band broadened and four Lorentzians appeared, denoting the individual behaviour of the fully clamped and the partially clamped monolayers. (d) The 2D band analysis showed the appearance of an additional band caused by strain, representing the individual 2D bands of each monolayer. The fully clamped monolayer experienced a maximum $\varepsilon = 14\%$, while the partially clamped monolayer experienced $\varepsilon = 2.21\%$.

clamped graphene was positioned under the laser spot of the Raman such that the TIM could be simultaneously actuated using two probe needles. A digital voltage source, Hameg HMP2020, heated the TIM with a power sweep from 0 W to 2.4 W.

3. Results and discussion

3.1. Stretching graphene of varying thicknesses

We started analyzing a bilayer sample by optical tracking, from which we extracted the original length of the flake, $L_o = 9.7\,\mu$m. At a maximum applied force of 330 μN, and based on visual displacement of the beams, the stretched flake showed an elongation of $\Delta L = 1.37\,\mu$m, denoting an achieved strain of $\varepsilon = \Delta L/L_o \approx 14\%$ (figure 2(a)). The optical images showed the gradual appearance of an edge after reaching $\varepsilon = 8.7\%$, suggesting that only one of the monolayers was properly clamped on both sides, and that slippage between both monolayers occurred upon straining. We confirmed this by observing the *in situ* shifts of the graphene's Raman spectra caused by increasing strain. It is well known that when probing the edge of graphene via Raman, the presence of the D-band is observed [23]. In our case, we noticed the initial appearance of that band while applying a force of ~200 μN (figure 2(b)), corresponding to the same strain where we observed the initial appearance of the edge during optical tracking. As the edge displaced and became more visible for the laser, the D-band showed increasing intensity with a maximum at 1356.9 cm^{-1}. Similarly, this was reversible, as the band gradually disappeared when returning to the relaxed state. Consequently, only the fully clamped monolayer experienced maximum strain in this experiment, while the other slipped and experienced a smaller strain. At this point, we can only speculate about the possible scenarios of why the complete clamping of the bilayer might have failed. One possibility is that one of the monolayers was shorter, preventing it from reaching both shuttles to be fully clamped. Alternatively, the glue might not have covered both edges of such a layer. We do not believe that the observed slippage is indicative for a fundamental failure of clamping bilayer graphene with our method.

From the Raman spectra, the G and 2D bands were individually analyzed. Initially the G-band was located at 1583.8 cm^{-1}, but displayed continuous redshift, resulting in 1579.2 cm^{-1} for $\varepsilon = 14\%$ (figure 3(a)). The complete evolution of the G-band, which can be found in figure 2 of the supplementary data, showed partial splitting and rise of

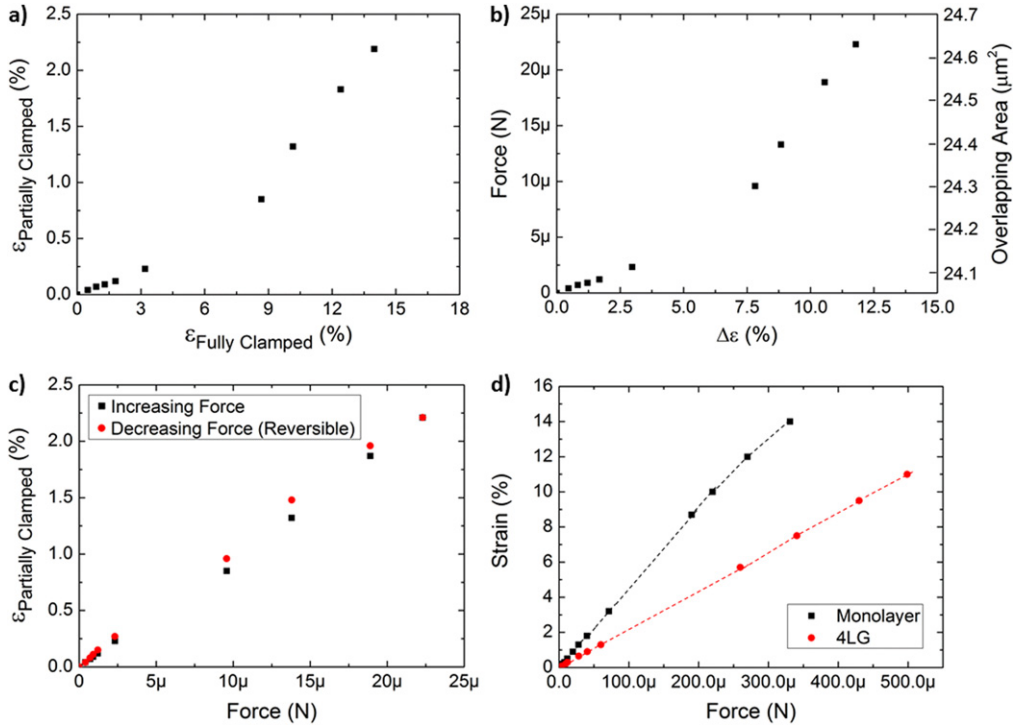

Figure 4. Slippage analysis between monolayers under extreme strain and stiffness comparison with multilayer. (a) We observed non-linear interaction between straining layers. (b) The strain difference between the monolayers, $\Delta\varepsilon$, is linked to the change in the interaction potential between both layers, as well as the location of the atoms. (c) When analyzing system reversibility, no changes in the spectra of the fully clamped monolayer were observed. However, when focusing on the partially clamped monolayer, a small hysteresis was observed in the spectra. The narrow hysteresis (or friction) loop implies a small amount of energy was lost as the slippage occurred when bringing the sample back to a relaxed state. (d) The force required to strain a monolayer to $\varepsilon = 14\%$ was 330 μN, however, such force would only induce a $\varepsilon = 7.5\%$ on a 4LG sample, denoting the higher stiffness of the latter.

different peaks. Previously, it was demonstrated that, when strained at $\varepsilon = 0.5\%$, the G-band of graphene splits into G^+ and G^- [24]. The individual G-band of each monolayer reacted separately because of their different strain values. When relaxed, the G-band of our bilayer showed two Lorentzian fits with maxima at 1583.8 cm^{-1} and 1589.3 cm^{-1} (figure 3(b)). The increase in strain was coupled to redshifts of both Lorentzians, eventual splitting, broadening, and dropping in intensity. At $\varepsilon = 0.5\%$, the G-band of the fully clamped monolayer divided into G^- at 1575.9 ± 03 cm^{-1} and G^+ at 1580.9 ± 02 cm^{-1}, as confirmed by a third Lorentzian (supplementary Data figure 2(d)). This suggested initial redshifts for the G^- and G^+ sub-bands of -15.9 $cm^{-1}/\%$ and -6.1 $cm^{-1}/\%$, respectively, which agrees with earlier findings [25]. At $\varepsilon = 8.7\%$, a fourth Lorentzian appeared, denoting the G-band splitting of the partially clamped monolayer (supplementary Data figure 2(i)). The G-band shape in figure 3(c) indicates an overlap of both monolayer's individual bands at their maximum experienced strain. The fully clamped monolayer showed its maxima at 1562.4 ± 03 cm^{-1} and 1592.2 ± 02 cm^{-1}, while the partially clamped at 1579.2 ± 04 cm^{-1} and 1597.3 ± 02 cm^{-1}. When analyzing the 2D band (figure 3(d)), we noticed that strain caused the appearance of an additional band, which we attribute to the individual 2D bands of each monolayer. At $\varepsilon = 14\%$, the spectra depicted two bands with redshifts of -58.9 cm^{-1} (partially clamped monolayer) and -372.4 cm^{-1} (fully clamped monolayer) with respect to the original 2D band, located at 2726.6 cm^{-1}. From these observations, we extracted a redshift of -26.6 $cm^{-1}/\%$ for the 2D band, in agreement with a previously reported redshift for the same band [26], which represented an experienced $\varepsilon = 2.21\%$ for the partially clamped monolayer.

The interaction between both monolayers as a function of strain is shown in figure 4(a). During straining, the weak inter-layer interaction enables the mechanism of slippage due to the presence of delocalized π electrons in the adjacent layers [27]. In our case, an estimated slipped distance of 1.19 μm was observed. This propensity for sliding also means that the local stacking of monolayer sheets can be disrupted. Similarly, we believe that the effect of tensile strain in the graphene causes a shift in the carbon-bonding configuration from sp^2 towards more sp^3, hence an increased interaction occurs between layers. However, our data is currently not detailed enough to reach this conclusion. The strain difference between the monolayers, $\Delta\varepsilon$, should be linked to the change in the interaction potential between the two layers, as well as the location of the atoms (figure 4(b)). Moreover, the reversibility of the mechanism was analyzed. The sample was controllably strained to its maximum strain and brought back to a relaxed state, and no changes in the spectra of the fully clamped monolayer were observed. Such a reversible and fast recovery property demonstrated the exceptional elasticity of graphene, which might be crucial for practical applications.

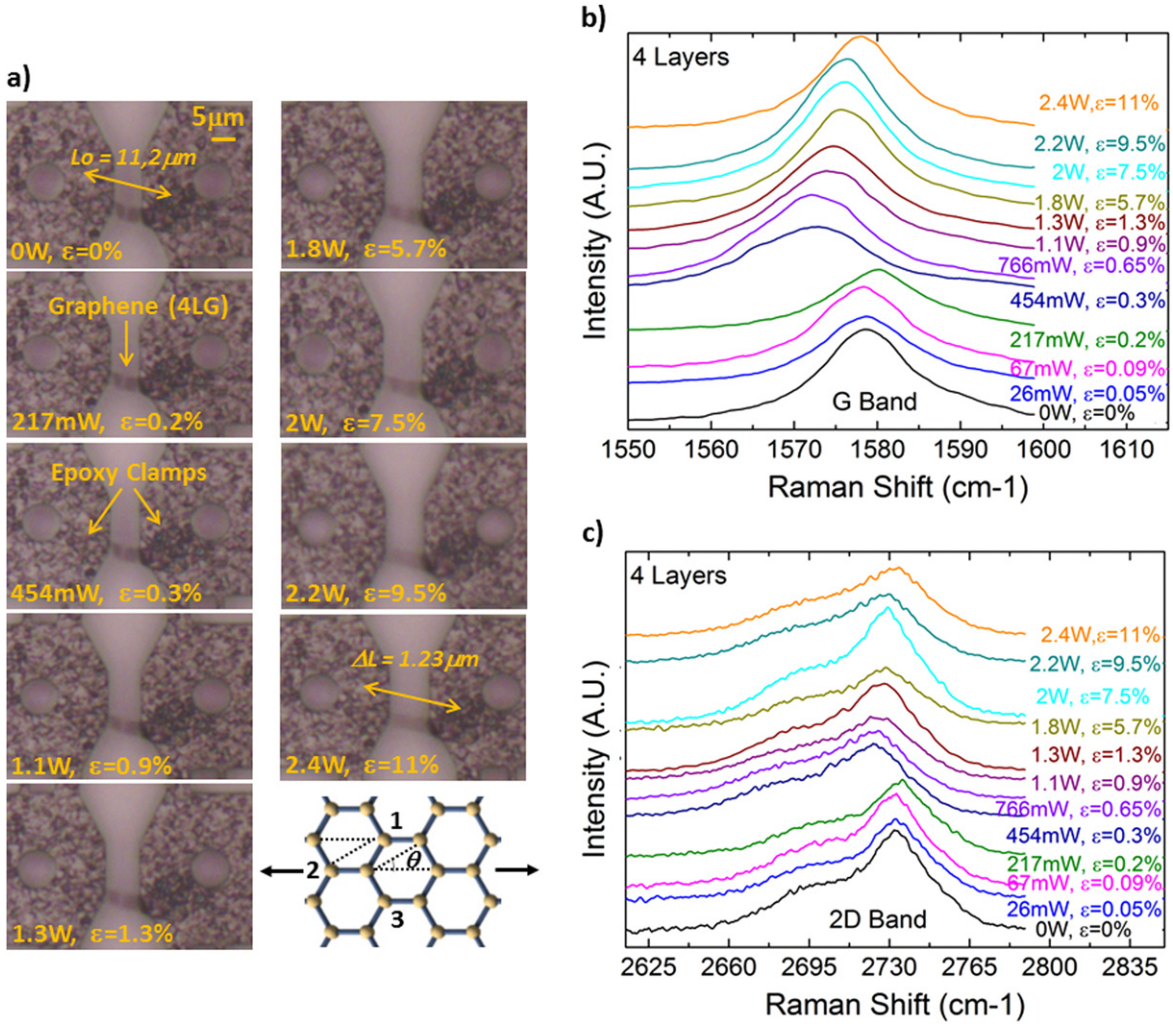

Figure 5. Highly strained multilayer. A four-layer graphene, 4LG, was strained with the same parameters. (a) The optical tracking of this sample is shown. Additionally, both the (b) G band and (c) 2D band were individually analyzed.

However, when focusing on the partially clamped monolayer, a small hysteresis was observed in the spectra, likely due to interlayer slippage. Figure 4(c) shows the obtained hysteresis loop, also referred to as the friction loop. The narrow loop implies a small amount of lost energy as the slippage occurred when bringing the sample back to a relaxed state. This corroborates the high lubricity of graphene that has been previously measured [28]. Similarly, earlier studies showed that ultra-low friction between is indeed caused by the incommensurate contact between the graphite layers [29]. Additionally, such controlled and reversible slippage resembled the experiments performed by Cumings *et al* [30], where the core tubes of multiwalled carbon nanotubes were telescoped outward, realizing low-friction.

To further exploit the behavior of highly stressed graphene, we repeated the experiments on a four-layer (4LG) sample. The confirmation of the number of layers is shown in figure 3 of the supplementary data. As expected, a smaller force was required to stretch the monolayer in comparison to the 4LG, as the latter was stiffer (figure 4(d)). For comparison, using a force of nearly 350 μN was enough to strain the monolayer by 14%, while the same force resulted in only 7.5% for the 4LG.

The optical tracking of the 4LG (figure 5(a)) revealed a maximum achieved strain of $\varepsilon = 11\%$. However, the Raman analysis showed different behavior in comparison with a highly strained monolayer. In 4LG, splitting the bands did not occur, and their redshift was much smaller. Its G-band redshifted from 1578.2 cm^{-1} to 1577.6 cm^{-1}, representing an average shift of -0.05 $cm^{-1}/\%$ (figure 5(b)). Similarly, its 2D band shifted from 2733.1 cm^{-1} to 2731.2 cm^{-1}, which represented an average shift of -0.17 $cm^{-1}/\%$ (figure 5(c)).

3.2. Comparing behaviors of stretched graphene samples

The average shifts of both the G-band and the 2D band shown by the 4LG were much smaller than that of the monolayer. Nevertheless, they were very similar to that of the previously reported 3LG [19], suggesting a general behaviour for highly stressed multilayer graphene (figures 6(a), (b)). As opposed to a monolayer where the G-band showed clear splitting due to strain, in the multilayer, splitting did not occur. Instead, the increase in strain was accompanied by a noticeable decrease

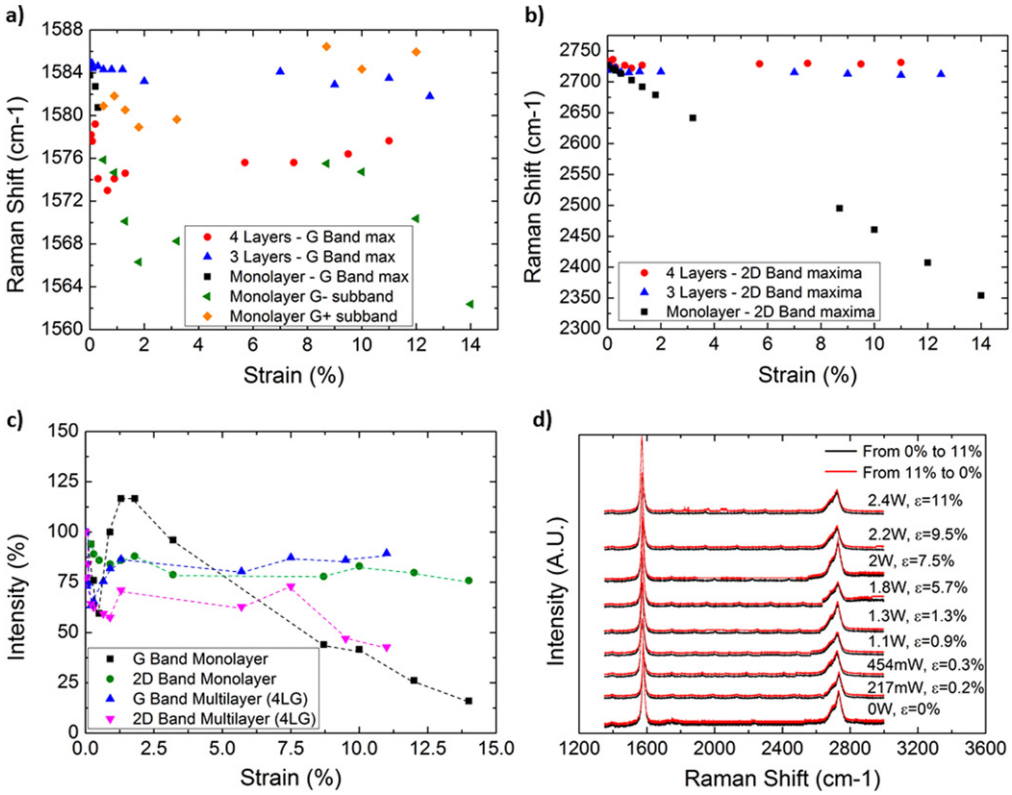

Figure 6. Comparison of behaviour between highly strained monolayer and multilayer. (a) The G band of multilayer graphene exhibited a very small Raman shift, as opposed to the monolayer, where the shift was more pronounced. Similarly, (b) the 2D band of the multilayer graphene remained almost static, while the monolayer displayed a noticeable shift. (c) The increase in strain was accompanied by a decrease in band intensity. In the case of a monolayer, an increase in strain resulted in a considerable decrease of intensity for the G-band and a minor decrease for the 2D band. In the case of the multilayer, however, the behaviour was the opposite. (d) Stretching the graphene from a relaxed state to a maximum strain and backwards resulted in the same Raman spectra, as shown by the absence of hysteresis, confirming the high elasticity of graphene.

in intensity and a smaller redshift. The 2D band of 4LG exhibited an average decrease of 4.8% in intensity per 1% strain, similar to that shown by the G-band of the monolayer. In the latter case, the average decrease in intensity was calculated to be 6% per 1% strain. On the other side, the G-band of the 4LG showed an average decrease of 1.26% in intensity per 1% strain, similar to the average decrease of the 2D band of a monolayer, which was measured to be 1.7% per 1% strain (figure 6(c)). In every case, these measurements were based on the maxima of the bands. Moreover, when the 4LG was strained from 0% to 11% and backwards, no hysteresis in the spectra were observed (figure 6(d)), corroborating the reversibility previously observed for monolayer graphene and the 3LG [19].

As observed in our earlier-reported results [19], it is due the C_{3v} group symmetry of graphene that the applied tensile strain distinguishes between the strain felt by the three bonds of graphene (denoted as 1, 2 and 3 in figure 5(a)). We believe that the asymmetric response of the three bonds of C_{3v} group symmetry gave rise to the behaviours reported here. The level of the strain and the strain energy of each C–C bond must differ with the relative direction between strain and crystal orientation. It is, therefore, not surprising that mechanical strain induces phonon-band splitting [31]. The bond order-length-strength (BOLS) correlation theory [31–34] helped us to once again calculate the individual elongations of the bonds in monolayer graphene. There are two extreme conditions defined by the angle $\theta = 0°$ or $\theta = 30°$, figure 5(a)). On one hand, when $\theta = 0°$, the strain is along bond 2, $\varepsilon 1 = \varepsilon 3 = \lambda\varepsilon 2 < \varepsilon 2$, where $\lambda = 0.31$ for the upper branch and $\lambda = 1.0$ for the lower branch. This means that bonds 1 and 3 are elongated by 31% compared to bond 2 when strain is along that bond. If we use 0.142 nm as the length for C–C bond in graphene [31] under the relaxed state, it would mean that bond 2 reached a length of 0.161 nm for $\varepsilon = 14\%$ achieved in our monolayer experiment, while bonds 1 and 3 reached 0.148 nm. Straining at $\theta = 0°$ should correspond to band splitting, which has been observed in monolayer graphene. On the other hand, when strain is perpendicular to bond 3, at $\theta = 30°$, the strain is $\varepsilon 1 = \varepsilon 2 > \varepsilon 3 \sim 0$ and therefore there should be a branch retaining the original frequency as $\varepsilon 3 \sim 0$. We believe that was the case in our 4LG, since no significant redshift for the 2D band was observed. Moreover, the diverse scattering paths (given by those three C–C bonds) for electrons and holes between the Dirac cones at the K and K′ points offer equal impact to the intensity of the 2D band. Therefore, if the symmetry is lost, a reduction of the intensity would be expected as a function of strain [35].

4. Conclusions

By using Raman spectroscopy to analyze graphene [36], we demonstrated the behaviour and main differences between highly strained monolayers and multilayers. The results confirmed the feasibility of using an in-plane tensile device to uniaxially stress graphene of varying thicknesses to extreme strains. As stated in our earlier results [19], the combination of the high–force output, long displacements, the high control provided by our MEMS device and the strong epoxy clamps were the main reasons for achieving high strains. The comparable results observed for 3LG and 4LG convinces us that the behaviour of samples with a larger number of layers could be predicted. We expect such larger numbers to result in small redshifts for the 2D band and an overall decrease of intensity, as long as all the layers are being strained. However, working with thicker samples could make the clamping more difficult, as the glue might not reach every layer. This given the fact that all layers might not have free edges where the glue could bind. Nonetheless, we believe our results can provide a deeper understanding of graphene's behaviour as a function of strain and varying thickness. These results might open doors to novel applications in electronics, optical devices and hydrogen-storage technologies. In addition, the observed slippage behaviour might be of high interest for further understanding of nanoscale friction and superlubricity, while providing insight for the design of novel lubricants.

Acknowledgments

The authors would like to thank the members of the Micro and Nano Engineering group for fruitful discussions. The technical staff of the DIMES Technology Center and Kavli Nanolab at TU Delft are also acknowledged. This work was supported by NanoNextNL, a micro- and nano-technology consortium of the government of the Netherlands and 130 partners. Similarly, the research leading to these results received funding from the European Research Council under the European Union's Seventh Framework Programme (FP/2007-2013)/ERC Grant Agreement 335879.

References

[1] Novoselov K S, Geim A K, Morozov S V, Jiang D, Zhang Y, Dubonos S V, Grigorieva I V and Firsov A A 2004 Electric field effect in atomically thin carbon films *Science* **306** 666–9

[2] Geim A K and Novoselov K S 2007 The rise of graphene *Nat. Mater.* **6** 183–91

[3] de Andres P L and Verges J A 2008 First-principles calculation of the effect of stress on the chemical activity of graphene *Appl. Phys. Lett.* **93** 171915

[4] Yang M, Nurbawono A, Zhang C, Wu R Q, Feng Y P and Ariando 2011 Manipulating absorption and diffusion of H atom on graphene by mechanical strain *Aip. Adv.* **1** 032109

[5] Levy N, Burke S A, Meaker K L, Panlasigui M, Zettl A, Guinea F, Neto A H C and Crommie M F 2010 Strain-induced pseudo-magnetic fields greater than 300 tesla in graphene nanobubbles *Science* **329** 544–7

[6] Low T and Guinea F 2010 Strain-induced pseudomagnetic field for novel graphene electronics *Nano Lett.* **10** 3551–4

[7] Pan W, Xiao J L, Zhu J W, Yu C X, Zhang G, Ni Z H, Watanabe K, Taniguchi T, Shi Y and Wang X R 2012 Biaxial compressive strain engineering in graphene/boron nitride heterostructures *Sci. Rep.-UK* **2** 893

[8] Tomori H, Kanda A, Goto H, Ootuka Y, Tsukagoshi K, Moriyama S, Watanabe E and Tsuya D 2011 Introducing nonuniform strain to graphene using dielectric nanopillars *Appl. Phys. Express* **4**

[9] Bunch J S, Verbridge S S, Alden J S, van der Zande A M, Parpia J M, Craighead H G and McEuen P L 2008 Impermeable atomic membranes from graphene sheets *Nano Lett.* **8** 2458–62

[10] Peng X H and Velasquez S 2011 Strain modulated band gap of edge passivated armchair graphene nanoribbons *Appl. Phys. Lett.* **98** 023112

[11] Rechtsman M C, Zeuner J M, Tunnermann A, Nolte S, Segev M and Szameit A 2013 Strain-induced pseudomagnetic field and photonic Landau levels in dielectric structures *Nat. Photonics* **7** 153–8

[12] Lee C, Wei X D, Kysar J W and Hone J 2008 Measurement of the elastic properties and intrinsic strength of monolayer graphene *Science* **321** 385–8

[13] Bao W Z, Miao F, Chen Z, Zhang H, Jang W Y, Dames C and Lau C N 2009 Controlled ripple texturing of suspended graphene and ultrathin graphite membranes *Nat. Nanotechnol.* **4** 562–6

[14] Kim K S, Zhao Y, Jang H, Lee S Y, Kim J M, Kim K S, Ahn J H, Kim P, Choi J Y and Hong B H 2009 Large-scale pattern growth of graphene films for stretchable transparent electrodes *Nature* **457** 706–10

[15] Chen C Y, Rosenblatt S, Bolotin K I, Kalb W, Kim P, Kymissis I, Stormer H L, Heinz T F and Hone J 2009 Performance of monolayer graphene nanomechanical resonators with electrical readout *Nat. Nanotechnol.* **4** 861–7

[16] Ferralis N 2010 Probing mechanical properties of graphene with Raman spectroscopy *J. Mater. Sci.* **45** 5135–49

[17] Klimov N N, Jung S, Zhu S Z, Li T, Wright C A, Solares S D, Newell D B, Zhitenev N B and Stroscio J A 2012 Electromechanical properties of graphene drumheads *Science* **336** 1557–61

[18] Fu X W *et al* 2011 Strain dependent resistance in chemical vapor deposition grown graphene *Appl. Phys. Lett.* **99** 213107

[19] Heuck F 2010 Developing and analysing sub-10 um fluidic systems with integrated electrodes for pumping and sensing in nanotechnology applications *PhD Thesis*

[20] Perez Garza H H, Ghatkesar M and Staufer U 2013 Combined AFM-nanopipette cartridge system for actively dispensing femtolitre droplets *J. Micro-Bio Robotics* **8** 33–40

[21] De-en J, Sumpter B G and Dai S 2007 Unique chemical reactivity of a graphene nanoribbon's zigzag edge *J. Chem. Phys.* **126** 134701

[22] Schneider G F, Calado V E, Zandbergen H, Vandersypen L M K and Dekker C 2010 Wedging transfer of nanostructures *Nano Lett.* **10** 1912–6

[23] Gupta A K, Russin T J, Gutierrez H R and Eklund P C 2009 Probing graphene edges via Raman scattering *Acs. Nano.* **3** 45–52

[24] Mohiuddin T M G *et al* 2009 Uniaxial strain in graphene by Raman spectroscopy: G peak splitting, Gruneisen parameters, and sample orientation *Phys. Rev.* B **79** 205433

[25] Huang M Y, Yan H G, Heinz T F and Hone J 2010 Probing strain-induced electronic structure change in graphene by Raman spectroscopy *Nano. Lett.* **10** 4074–9

[26] Ni Z H, Yu T, Lu Y H, Wang Y Y, Feng Y P and Shen Z X 2009 Uniaxial strain on graphene: Raman spectroscopy study and bandgap opening *ACS Nano.* **3** 2301–5

[27] Hasegawa M, Nishidate K and Iyetomi H 2007 Energetics of interlayer binding in graphite: the semiempirical approach revisited *Phys. Rev.* B **76** 115424
[28] van Wijk M M, Dienwiebel M, Frenken J W M and Fasolino A 2013 Superlubric to stick-slip sliding of incommensurate graphene flakes on graphite *Phys. Rev.* B **88** 235423
[29] Dienwiebel M, Verhoeven G S, Pradeep N, Frenken J W M, Heimberg J A and Zandbergen H W 2004 Superlubricity of graphite *Phys. Rev. Lett.* **92** 126101
[30] Cumings J and Zettl A 2000 Low-friction nanoscale linear bearing realized from multiwall carbon nanotubes *Science* **289** 602–4
[31] Yang X X, Li J W, Zhou Z F, Wang Y, Yang L W, Zheng W T and Sun C Q 2012 Raman spectroscopic determination of the length, strength, compressibility, Debye temperature, elasticity, and force constant of the C–C bond in graphene *Nanoscale* **4** 502–10
[32] Sun C Q 2007 Size dependence of nanostructures: impact of bond order deficiency *Prog. Solid State Ch.* **35** 1–159
[33] Sun C Q, Bai H L, Tay B K, Li S and Jiang E Y 2003 Dimension, strength, and chemical and thermal stability of a single C–C bond in carbon nanotubes *J. Phys. Chem.* B **107** 7544–6
[34] Sun C Q, Sun Y, Nie Y G, Wang Y, Pan J S, Ouyang G, Pan L K and Sun Z 2009 Coordination-resolved C–C bond length and the C 1s binding energy of carbon allotropes and the effective atomic coordination of the few-layer graphene *J. Phys. Chem.* C **113** 16464–7
[35] Popov V N and Lambin P 2013 Theoretical Raman intensity of the G and 2D bands of strained graphene *Carbon* **54** 86–93
[36] Ferrari A C and Basko D M 2013 Raman spectroscopy as a versatile tool for studying the properties of graphene *Nat. Nanotechnol.* **8** 235–46